ANOMALIES AND PRECISION — LATEST CMS B-PHYSICS HIGHLIGHTS*

Muhammad Alibordi

on behalf of the CMS Collaboration

Faculty of Physics, University of Warsaw, Pasteura 5, Warsaw, Poland

Received 29 March 2024, accepted 1 July 2024, published online 5 August 2024

In this note, we will discuss some of the latest high-precision measurements performed by the Compact Muon Solenoid (CMS) experiment in the B-physics sector of high energy physics.

DOI:10.5506/APhysPolBSupp.17.5-A21

1. Introduction

CMS is a general-purpose detector, and it comprises a tracker, an electromagnetic calorimeter, and a hadron calorimeter surrounded by a solenoid magnetic coil, which provides $\sim 4\,\mathrm{T}$ magnetic field, further covered by a muon chamber. The proton beams delivered from the Large Hadron Collider (LHC) collide at the heart of the CMS detector. To identify and record interesting physics events, a two-tier trigger system is employed: a hardware-based Level-1 (L1) trigger and a software-based High-Level Trigger (HLT) [1]. The detector performance of the CMS is highly optimized, resulting in excellent reconstruction efficiency of the desired particles. Utilizing these advantages, CMS has already shown precise measurements in the bottom physics sector. In the current proceedings, we will demonstrate some of the precise measurements related to the spectroscopy of hadron physics, the lepton flavor universality violation, and the studies in discrete symmetries performed by the CMS Collaboration.

2. Spectroscopy

2.1. $\eta \to \mu^+\mu^-\mu^+\mu^-$

The Dalitz decay of the $\eta(J^{PC} = 0^{-+})$ meson of mass 547.9 MeV into four muons proceeds via the electromagnetic coupling of the pseudoscalar

* Presented at the 30th Cracow Epiphany Conference on *Precision Physics at High Energy Colliders*, Cracow, Poland, 8–12 January, 2024.

meson to the photon, where the photons are internally converted to pairs of leptons. Observation of the $\eta \to 4\mu$ decay enhances the precision of the Standard Model of particle physics, and simultaneously offers sensitivity to a set of models corresponding to new physics scenarios [2]. In CMS, we first observed the double-Dalitz decay of the η meson, $\eta \to \mu^+\mu^-\mu^+\mu^-$, by making the usage of the $\sqrt{s} = 13$ TeV proton–proton (pp) collision data collected by the CMS detector in the years 2017 and 2018 corresponding to a total integrated luminosity of 101 fb^{-1}. The branching fraction of the $\eta \to \mu^+\mu^-\mu^+\mu^-$ decay, $\mathcal{B}(\eta \to 4\mu)$, is estimated relative to the known branching fraction of the $\eta \to 2\mu$ decay, $\mathcal{B}(\eta \to 2\mu) = (5.8 \pm 0.8) \times 10^{-6}$. In order to select events corresponding to the above channels, the standard dimuon triggers are utilized. These triggers require one muon with transverse momentum p_{T} larger than 12(15) GeV at L1 in 2017 (2018) and of 17 GeV at HLT. The second muon has $p_{\mathrm{T}} \leq 5(7)$ GeV at level one in 2017 (2018) and 8 GeV at HLT. In order to improve the signal-over-background ratio, oppositely-charged muons originating from common vertex are used for the reconstruction of the 2μ (4μ) final state of the η meson within the η meson mass range of 0.518–0.578 (0.46–0.90) GeV. As shown in Fig. 1, left, the observed signal peak of the η meson in the signal mass window 0.53–0.57 GeV is fitted with a single-sided Crystal–Ball function, and the background ($\eta \to (\pi^+\pi^-\mu^+\mu^-, \mu^+\mu^-\gamma, \pi^+\pi^-\pi^0, \pi^0\pi^0\pi^0, \pi^+\pi^-\gamma)$) with a threshold function proportional to $(m_{4\mu} - 4m_\mu)^\beta$, by making the usage of binned maximum likelihood fit, where m_μ is the mass and β is the free parameter. The clear yield of $N_{4\mu} = 49.6 \pm 8.1$ number of signal events over 16.6 ± 0.6 background events, corresponds to a statistical significance in excess of 5 standard deviations, estimated by utilizing a log-likelihood

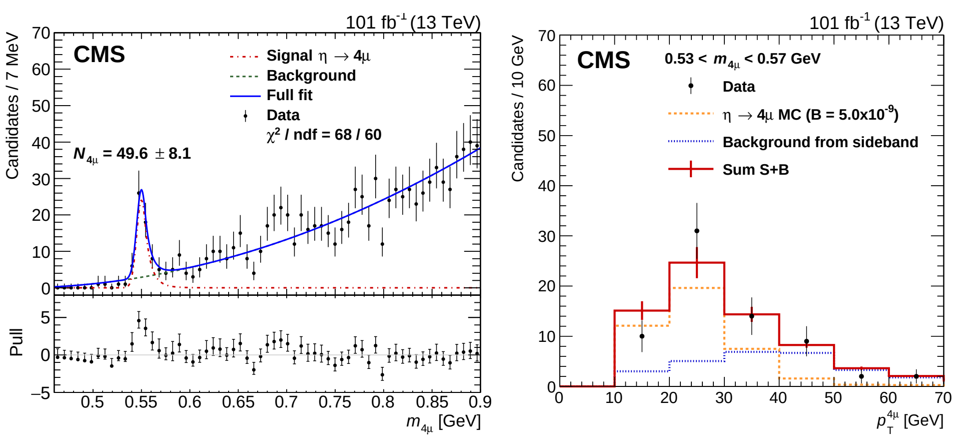

Fig. 1. Invariant mass distribution of the $\eta \to \mu^+\mu^-\mu^+\mu^-$ process (left) and comparison of the p_{T} between the signal, and the background (right) [2].

ratio test with a saturated model [3], under signal-plus-background (S+B) hypothesis compared to the background-only assumption. The agreement between measured $p_{\rm T}$ spectrum from the data and the predicted distribution from the simulated events is shown in Fig. 1, right. The branching faction of the decay $\eta \to 4\mu$ is determined using

$$\frac{\mathcal{B}_{4\mu}}{\mathcal{B}_{2\mu}} = \frac{N_{4\mu}}{\sum_{i,j} N_{2\mu}^{i,j} \frac{A_{4\mu}^{i,j}}{A_{2\mu}^{i,j}}}\,, \tag{1}$$

where the $N_{4\mu}$ is the total signal yield of the $\eta \to 4\mu$ decay process, $N_{2\mu}^{i,j}$ are the signal yields of $\eta \to 2\mu$ in bins i, and j of the candidate η's $p_{\rm T}$ and rapidity, and $A_{n\mu}^{i,j}$ are the efficiencies. Given the known branching fraction of the $\eta \to 2\mu$ process, the obtained branching fraction of the newly observed decay $\eta \to 4\mu$ process is obtained to be

$$\mathcal{B}(\eta \to 4\mu) = [5.0 \pm 0.8(\text{stat.}) \pm 0.7(\text{syst.}) \pm 0.7(\mathcal{B}_{2\mu})] \times 10^{-9}\,, \tag{2}$$

where the last term is the uncertainty related to the branching fraction in $\mathcal{B}(\eta \to 4\mu)$, and the result is in agreement with the theoretical prediction $(3.98 \pm 0.15) \times 10^{-9}$.

2.2. $B_s^0 \to \mu^+\mu^-$

The rare decays of the B mesons are the sensitive probe of the BSM physics. The measurement of the properties of the $B_s^0 \to \mu^+\mu^-$ decay process obtained by using the *pp* collision data collected by the CMS detector in 2016–2018 corresponds to a total integrated luminosity of $\mathcal{L}_{\rm int} = 140$ fb^{-1}. Two oppositely-charged muons are used to form the signals of the leptonic B meson decays, and in order to further improve the signal yield, several physics selections are applied. The known backgrounds are the $B^0 \to \mu^+\mu^-$ signals, partially reconstructed semileptonic backgrounds of the $B \to h^-\mu^+\nu(h\mu^+\mu^-)$ type, where the $h \in (\pi, K, p)$ represents a hadron, the peaking background $B \to h^+h^-$, and the combinatorial background. In order to extract the branching fraction, signal yield and the effective lifetime of the $_s^0 \to \mu^+\mu^-$ channels, such as $B^+ \to J/\psi K^+$, $B_s^0 \to J/\psi\phi(1020)$, are used as the control channels. The branching fraction of the decay process $B_s^0 \to \mu^+\mu^-(B^0 \to \mu^+\mu^-)$ is determined using

$$\mathcal{B}\left(B_s^0 \to \mu^+\mu^-\right) = \frac{N_s}{N_{\rm obs}^{B^+}} \frac{f_u}{f_s} \frac{\epsilon_{\rm tot}^{B^+}}{\epsilon_{\rm tot}} \mathcal{B}\left(B^+ \to J/\psi K^+\right) \mathcal{B}\left(J/\psi \to \mu^+\mu^-\right)\,, \tag{3}$$

where the uncertainty on the fragmentation fraction (for B^0, the ratio is $\frac{f_d}{f_u}$) depends on the normalization channel $B^0_s \to J/\psi\phi(1020)$

$$\begin{aligned} \mathcal{B}\left(B^0_s \to \mu^+\mu^-\right) &= \left[3.83^{+0.38}_{-0.36}(\text{stat.})^{0.19}_{-0.16}(\text{syst.})^{0.14}_{-0.13}(f_s/f_u)\right] \times 10^{-9}\,, \\ \tau_{\mu^+\mu^-} &= \left[1.83^{+0.23}_{-0.20}(\text{stat.})^{0.04}_{0.04}(\text{syst.})\right]\ \text{ps}\,. \end{aligned} \tag{4}$$

A 2D unbinned maximum likelihood (UML) fit is performed to obtain the effective lifetime of the decay process $B^0_s \to \mu^+\mu^-$, in which the decay time efficiencies $\epsilon(t)$ corresponding to each type of the background are also considered. The results of the branching fraction and the effective lifetime obtained from the UML fit are shown in Eq. (4). Figure 2, left shows the profile likelihood as a function of the branching fraction in the corresponding decays, Fig. 2 middle and Fig. 2, right show the UML fit to the invariant mass distribution and the effective lifetime distribution of the decay process $B^0_s \to \mu^+\mu^-$ [4].

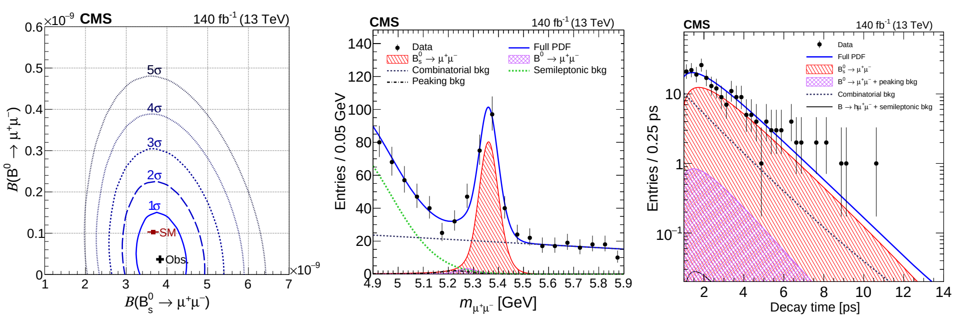

Fig. 2. Left: The 2D contour of the profile likelihood as a function of the branching fraction of the $B^0_s \to \mu^+\mu^-$ and $B^0 \to \mu^+\mu^-$ decays, enclose the 1–5σ region, where $1, 2$, and 3σ regions correspond to 68.3, 95.4, and 99.7% of confidence levels respectively. Middle and right: Two-dimensional UML fit to the invariant mass distribution and effective lifetime of the decay process $B^0_s \to \mu^+\mu^-$ respectively. The solid blue curves represent the final fit projection, whereas the individual components are represented by the dashed lines (backgrounds) and hatched histograms (signals) [4].

3. Lepton flavour universality violation

3.1. $\tau \to 3\mu$

The branching fraction of the lepton flavor violating decay process $\tau \to 3\mu$ is around $\mathcal{B}(\tau \to 3\mu) \sim \mathcal{O}(10^{-10})$ in various BSM scenarios [5]. The measurement of $\mathcal{B}(\tau \to 3\mu)$ is determined using the pp collision data collected in 2017 and in 2018 which corresponds to a total integrated luminosity of 97.7 fb^{-1}, and the obtained result is further combined with previously measured result of 2016 data [6]. The measurement exploits the production of tau lepton in both heavy-flavor decays, such as, $D_s^+ \to \tau^+\nu_\tau, B^+/B^0 \to \tau + X$, and also in W-boson decays, $W^+ \to \tau^+\nu_\tau$. The decay process $D_s^+ \to \phi\pi^+ \to \mu^+\mu^-\pi^+$ is used as the normalization channel in the heavy-flavor decays. The three muon yields in each case are related to the branching fraction, as

$$N_{3\mu(D)} = N_{\mu\mu\pi} \frac{\mathcal{B}\left(D_s^+ \to \tau^+\nu_\tau\right)}{\mathcal{B}\left(D_s^+ \to \phi\pi^+ \to \mu^+\mu^-\pi^+\right)} \frac{\mathcal{A}_{3\mu(D)}}{\mathcal{A}_{\mu\mu\pi}} \frac{\epsilon^{\text{reco}}_{3\mu(D)}}{\epsilon^{\text{reco}}_{\mu\mu\pi}} \frac{\epsilon^{2\mu\text{trig}}_{3\mu(D)}}{\epsilon^{2\mu\text{trig}}_{\mu\mu\pi}} \mathcal{B}(\tau \to 3\mu)\,,$$

$$N_{3\mu(B)} = N_{\mu\mu\pi} f \frac{\mathcal{B}\left(B \to \tau^+X\right)}{\mathcal{B}\left(\mathrm{B} \to D_s^+ + X\right)\mathcal{B}\left(D_s^+ \to \phi\pi^+ \to \mu^+\mu^-\pi^+\right)}$$
$$\times \frac{\mathcal{A}_{3\mu(B)}}{\mathcal{A}_{\mu\mu\pi}} \frac{\epsilon^{\text{reco}}_{3\mu(B)}}{\epsilon^{\text{reco}}_{\mu\mu\pi}} \frac{\epsilon^{2\mu\text{trig}}_{3\mu(B)}}{\epsilon^{2\mu\text{trig}}_{\mu\mu\pi}} \mathcal{B}(\tau \to 3\mu)\,,$$

$$N_{3\mu(W)} = \mathcal{L}\sigma(pp \to W + X)\mathcal{B}(W \to \tau\nu_\tau)\mathcal{A}_{3\mu(W)}\epsilon_{3\mu(W)}\mathcal{B}(\tau \to 3\mu)\,,$$

where $\mathcal{A}$ is the detector acceptance, $\epsilon^{\text{reco(trig)}}$ is the selection (trigger) efficiency, f is the ratio of the cross sections, $f = (pp \to B + X)\mathcal{B}(B \to D_s^+ + X)/\sigma(pp \to D_s^+ + X)$. The signal-to-background ratio is optimized using the Boosted Decision Tree (BDT) algorithm and, finally, three mass resolution categories are introduced, $A : \sigma_m = 12$ MeV, $\sigma_m/m < 0.07\%$, $B : \sigma_m = 19$ MeV, $0.07 < \sigma_m/m < 1.05\%$, $C : \sigma_m = 25$ MeV, $\sigma_m/m > 1.05\%$. The signal region for each category includes the candidates with trimuon invariant masses within twice the mass resolution. A background-only fit is performed, and the observed (expected) upper limit on the branching fraction from the data of 2017–2018, which is then further combined with 2016, are C.L. — 90% : $2.9(2.4) \times 10^{-8}$, and C.L. — 95% : $3.6(3.0) \times 10^{-8}$ (Fig. 3).

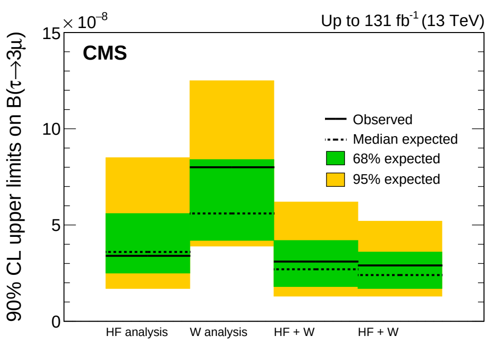

Fig. 3. Observed and expected upper limit on $\mathcal{B}(\tau \to 3\mu)$ at 90% C.L., from the heavy-flavor analysis and the W-boson analysis, the combination of the two analyses, and the combination with the result of the 2016 data [6].

3.2. $R(J/\psi)$: $B_c^+ \to J/\psi\tau^+\nu_\tau$

The measurement of $R(J/\psi)$ in the semitauonic channel $B_c^+ \to J/\psi\tau^+\nu_\tau$ is performed by exploiting the ratio of the branching fractions

$$R(J/\psi) = \frac{\mathcal{B}\left(B_c^+ \to J/\psi\tau^+\nu_\tau\right)}{\mathcal{B}\left(B_c^+ \to J/\psi\mu^+\nu_\mu\right)}\,, \tag{5}$$

where $J/\psi \to \mu^+\mu^-$, $\tau^+ \to \mu^+\nu_\mu\nu_\tau$, and in both cases, the final state comprises three muons, while using 2018 pp collision data corresponding to 59.7 fb^{-1} integrated luminosity. The events are selected with three muons, the requirement of the transverse momentum on the leading muon is $p_{\mathrm{T}} > 5$ GeV, the sub-leading muon is $p_{\mathrm{T}} > 3$ GeV, and no p_{T} requirement for sub-sub-leading muon. Two oppositely charged muons must originate from the common vertex of the J/ψ, and the muon, which is not originating from such a vertex is referred to as the third muon in the event. Several selection criteria are also applied in order to increase signal-over-background ratio, most importantly three observables with the highest discriminating power, namely the squared four-momentum transfer to the lepton system, $q^2 = (p_{B_c^+} - p_{J/\psi})^2$, significance of the 3D impact parameter IP3D/σ_{IP3D}, and the transverse decay length significance $L_{xy}/\sigma_{L_{xy}}$. The $p_{B_c^+}$ is defined as the $p_{B_c^+} = m_{B_c^+}/m_{3\mu}^{\mathrm{vis}} \cdot p_{3\mu}^{\mathrm{vis}}$, where $m_{3\mu}^{\mathrm{vis}}$ and $p_{3\mu}^{\mathrm{vis}}$ are the mass and four-momentum of the visible decay products (3μ). Figure 4 shows how the discriminators could clearly separate the signal from the different backgrounds, such as fakes, $J/\psi(\mu^+\mu^-) + h(h \in \pi, K)$ or $H_b \to J/\psi(\mu^+\mu^-) + \mu^+$. The measured value of $R(J/\psi)$ is found to be

$$R(J/\psi) = 0.17^{0.18}_{-0.17}(\mathrm{stat.})^{+0.21}_{-0.22}(\mathrm{syst.})^{0.19}_{-0.18}(\mathrm{theo.})\,. \tag{6}$$

This result is within 0.3σ (1.3σ) of the result from SM [8] (LHCb [9]).

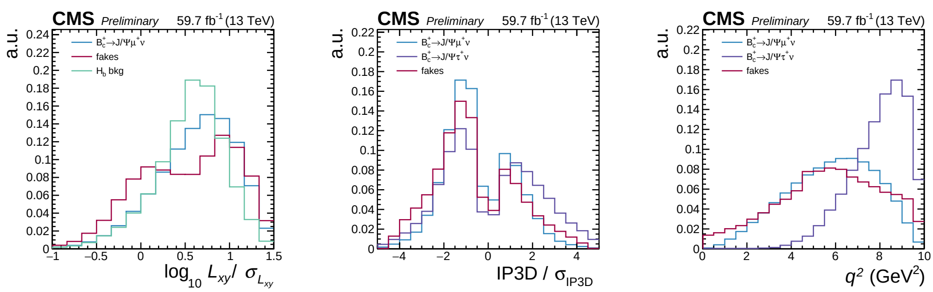

Fig. 4. The three discriminators with the highest discriminating power, transverse decay length significance (left), significance of 3D impact parameter (middle), and the four-momentum transfer to the lepton system (right) [7].

3.3. $R(K): B^{\pm} \to K^{\pm}\ell^{+}\ell^{-}$

Limited by the statistical uncertainty in the electron channel, the measurement of the $R(K)$ utilizes pp collisions data corresponding to integrated luminosity of $41.6 \pm 1.0\ \text{fb}^{-1}$ (2018). The measurement of $R(K)$ is found through the double ratio

$$R(K)\left(q^2\right) = \frac{\mathcal{B}\left(B^+ \to K^+\mu^+\mu^-\right)\left(q^2\right)}{\mathcal{B}\left(B^+ \to J/\psi(\mu^+\mu^-)K^+\right)} \Big/ \frac{\mathcal{B}\left(B^+ \to K^+e^+e^-\right)\left(q^2\right)}{\mathcal{B}\left(B^+ \to J/\psi\left(e^+e^-\right)K^+\right)}\,. \quad (7)$$

Several physics selections are applied based on the kinematic observables to enhance the signal yield in both electron and muon channels. The invariant mass distribution in both electron and muon channels shown in Fig. 5 depicts the fit of the mass distribution with complimentary probability distribution functions for both signal and background respectively. A dedicated low momentum algorithm (LP) is devised to deal with the systematic uncertainties of the electron, and the measurement is performed in three different resonance bins of the q^2. The measured value of the $R(K)$ and the integrated branching fraction in the muon channel are found to be

$$R(K) = 0.78^{+0.47}_{-0.23}\,, \qquad \mathcal{B}\left(K^{\pm}\mu^+\mu^-\right) = (12.42 \pm 0.68) \times 10^{-8}\,. \quad (8)$$

The uncertainties in the results demonstrate both statistical and systematic uncertainty [10].

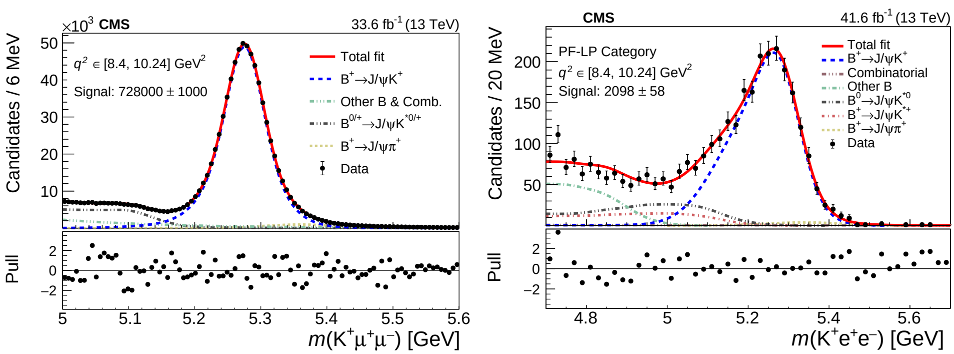

Fig. 5. (Color online) The fitted invariant mass distribution in both muon and electron channels, where the total fit is projected as the solid red line and the components are in dashed lines [10].

4. Studies of discrete symmetries

4.1. $\phi_s: B^0_s \to J/\psi\phi(1020)$

The measurement of the CP-violating weak phase ϕ_s in the $B^0_s \to J/\psi\phi$ channel is highly sensitive to the BSM physics. The value of ϕ_s is extracted by performing a flavor-tagged time-dependent angular analysis using pp collision data collected in the 2017–2018 data-taking period corresponding to a total integrated luminosity of 96.4 fb^{-1} at $\sqrt{s} = 13$ TeV. The flavor tagging is required to identify the initial state[1], and the angular analysis is required to disentangle the mixing of the odd and even CP flavor states in the decay products. An opposite side DNN-based flavor tagging algorithm is employed to infer the probability of identification of the initial flavor of B_s^0 or $\bar{B}_s^0$. The determined maximum attainable flavor tagging efficiency is $\sim 50\%$, where the event selection is optimized using a genetic algorithm. A multidimensional unbinned maximum likelihood fit model is employed in order to extract the values of the weak phase ϕ_s, the decay width difference $\Delta\Gamma_s$, the oscillation frequency Δm_s, and the direct CP-violating parameter $|\lambda|$. The model inputs are the invariant mass distribution $m_{B_s^0}$ of the B_s^0 candidate, the decay time $c\tau$, the decay time uncertainty $\Delta c\tau$, per event mistag probability ω, the tag decision ξ, the three angles, the efficiency of the decay time $\epsilon(c\tau)$, and the angular efficiency $\epsilon(\Theta)$. The three angles (Θ) are defined in the transversity basis of B_s^0 decay frame, namely the polar(θ_T), and azimuthal angle (ϕ_T) of the final-state particle μ^+, in the rest frame of the intermediate decay product of J/ψ mesons rest frame, and the helicity angle (ψ_T) of K^+, in the rest frame of the decay product of $\phi(1020)$ mesons rest frame. The measured results are $\phi_s = -11 \pm 50\,(\mathrm{stat.}) \pm 10\,(\mathrm{syst.})$ mrad,

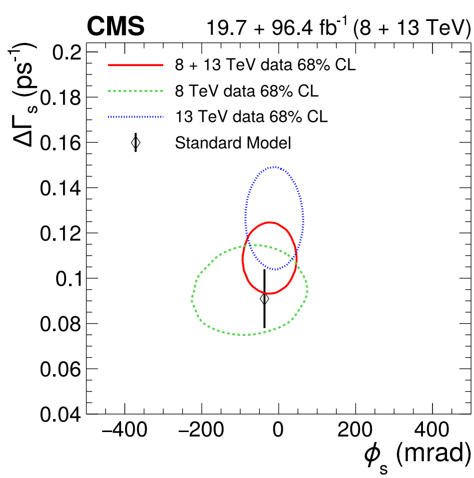

Fig. 6. The two-dimensional likelihood contours at 68% C.L. in the ϕ_s–$\Delta\Gamma_s$ plane, for the CMS 8 TeV (dashed line), 13 TeV (dotted line), and combined (solid line) results. The SM prediction is shown with the diamond marker [11].

[1] Due to B_s^0–$\bar{B}_s^0$ mixing, the initial state is not predefined.

$\Delta\Gamma_s = 0.114 \pm 0.014\,(\text{stat.}) \pm 0.007\,(\text{syst.})\ \text{ps}^{-1}$, $\Delta m_s = 17.51 \pm^{+0.10}_{-0.09}\,(\text{stat.}) \pm 0.03\,(\text{syst.})\,\hbar\,\text{ps}^{-1}$ and $|\lambda| = 0.972 \pm 0.026(\text{stat.}) \pm 0.003(\text{syst.})$. The 13 TeV results are further combined with the results of the weak phase and the decay width difference obtained at $\sqrt{s} = 8$ TeV, and the combined values are $\phi_s = -21 \pm 44\,(\text{stat.}) \pm 10\,(\text{syst.})$ mrad, and $\Delta\Gamma_s = 0.1032 \pm 0.0095\,(\text{stat.}) \pm 0.0048\,(\text{syst.})\ \text{ps}^{-1}$. As shown in the two dimensional ϕ_s–$\Delta\Gamma_s$ plane of Fig. 6, the results are consistent with the predicted values of the SM and the details of the references can be found in the Ref. [11].

4.2. $A_{\text{FB}}, F_{\text{L}} : B^+ \to K^{*+}\mu^+\mu^-$

The measurement of the forward–backward asymmetry (A_{FB}) and the longitudinal polarization (F_{L}) in the decay process $B^+ \to K^{*+}\mu^+\mu^-$ is utilizing 20 fb^{-1} of pp collision data collected at $\sqrt{s} = 8$ TeV. This is also an angular analysis where the angle θ_K is defined in the $K^{*+}(\to K^0_s\pi^+)$ rest frame and θ_l is defined in the $\mu^+\mu^-$ rest frame.

Physics selections are employed in order to increase the signal efficiency, and the values of the A_{FB} and the F_{L} are extracted by performing an binned maximum likelihood fit to the differential decay distribution. The multidimensional likelihood model does incorporate the invariant mass distribution, the angles , and the angular efficiency. The analysis is performed in three different bins of q^2, as shown in Fig. 7, where the vertical shaded regions correspond to the regions dominated by $B^+ \to K^{*+}J/\psi$ and $B^+ \to K^{*+}\psi(2S)$ decays. The results, shown with the black square, comprise both statistical and systematic uncertainties. Corresponding SM predictions are also displayed (blue dots) to show that the measurements are consistent with SM [12].

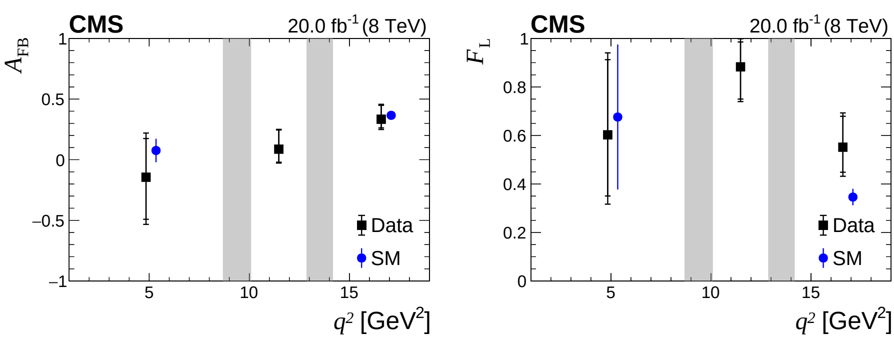

Fig. 7. (Color online) The measured values of A_{FB} (left) and the F_{L} (right) *versus* q^2 for $B^+ \to K^{*+}\mu^+\mu^-$ decays are shown with the filled squares, centered on the q^2 bin. The statistical (total) uncertainty is shown by inner (outer) vertical bars [12].

5. Conclusion

We have discussed some of the flagship analyses of the B-physics sector performed by the CMS experiment looking forward to unfolding various unknown features of flavor physics in the upcoming hi-luminosity era of the LHC.

This contribution is supported by the Ministry of Science and Higher Education (Poland) grant No. 2022/WK/14.

REFERENCES

[1] CMS Collaboration (A.M. Sirunyan *et al.*), *J. Instrum.* **15**, P10017 (2020).

[2] CMS Collaboration (A. Hayrapetyan *et al.*), *Phys. Rev. Lett.* **131**, 091903 (2023).

[3] S. Baker, R.D. Cousins, *Nucl. Instrum. Methods Phys. Res.* **221**, 437 (1984).

[4] CMS Collaboration (A. Tumasyan *et al.*), *Phys. Lett. B* **842**, 137955 (2023).

[5] CMS Collaboration, «Search for the lepton flavor violating $\tau \to 3\mu$ decay in proton–proton collisions at $\sqrt{s} = 13$ TeV», tech. rep., CERN, Geneva, 2023, submitted to *Phys. Lett. B*. All figures and tables can be found at `http://cms-results.web.cern.ch/cms-results/public-results/publications/BPH-21-005`, CMS Public Pages.

[6] CMS Collaboration (A.M. Sirunyan *et al.*), *J. High Energy Phys.* **2021**, 163 (2021).

[7] CMS Collaboration, «Test of lepton flavor universality violation in semileptonic B_c^+ meson decays at CMS», tech. rep., CERN, Geneva, 2023.

[8] J. Harrison, C.T.H. Davies, A. Lytle, *Phys. Rev. Lett.* **125**, 222003 (2020).

[9] LHCb Collaboration, *Phys. Rev. Lett.* **120**, 121801 (2018).

[10] CMS Collaboration, *Rep. Prog. Phys.* **87**, 077802 (2024), `arXiv:2401.07090 [hep-ex]`.

[11] CMS Collaboration, *Phys. Lett. B* **816**, 136188 (2021).

[12] CMS Collaboration (A.M. Sirunyan *et al.*), *J. High Energy Phys.* **2021**, 124 (2021).